CONF-9006242--2

LA-UR-90- 3180

Los Alamos National Laboratory is operated by the University of California for the United States Department of Energy under contract W-7405-ENG-36

TITLE: **PHOTOELECTRIC INJECTOR DESIGNS AT LOS ALAMOS NATIONAL LABORATORY**

LA-UR--90-3180

DE91 000369

AUTHOR(S): Bruce E. Carlsten
Richard L. Sheffield
Brian D. McVey

SUBMITTED TO: Bendor Workshop on Short Pulse High Current Cathodes
Bendor, France
June 18-22, 1990

By acceptance of this article, the publisher recognizes that the U.S. Government retains a nonexclusive, royalty-free license to publish or reproduce the published form of this contribution, or to allow others to do so, for U.S. Government purposes.

The Los Alamos National Laboratory requests that the publisher identify this article as work performed under the auspices of the U.S. Department of Energy

Los Alamos

Los Alamos National Laboratory
Los Alamos, New Mexico 87545

DISTRIBUTION OF THIS DOCUMENT IS UNLIMITED

FORM NO. 836 R4
ST NO 2629 5/81

PHOTOELECTRIC INJECTOR DESIGNS AT LOS ALAMOS NATIONAL LABORATORY*

Bruce E. Carlsten, Richard L. Sheffield, and Brian D. McVey

Los Alamos National Laboratory, MS-H825
Los Alamos, NM 87545

DISCLAIMER

This report was prepared as an account of work sponsored by an agency of the United States Government. Neither the United States Government nor any agency thereof, nor any of their employees, makes any warranty, express or implied, or assumes any legal liability or responsibility for the accuracy, completeness, or usefulness of any information, apparatus, product, or process disclosed, or represents that its use would not infringe privately owned rights. Reference herein to any specific commercial product, process, or service by trade name, trademark, manufacturer, or otherwise does not necessarily constitute or imply its endorsement, recommendation, or favoring by the United States Government or any agency thereof. The views and opinions of authors expressed herein do not necessarily state or reflect those of the United States Government or any agency thereof.

ABSTRACT

We will describe the photoelectric injector design philosophy and capabilities at Los Alamos National Laboratory. We will discuss our simulation ability and general considerations to minimize the space-charge and rf emittance growths. In particular, we will also outline a high frequency design without magnetic bunching and a low frequency design with magnetic bunching.

*Work supported and funded by the US Department of Defense, Army Strategic Defense Command, under the auspices of the US Department of Energy.

MASTER

DISTRIBUTION OF THIS DOCUMENT IS UNLIMITED

INTRODUCTION

We will describe the current photoelectric injector design philosophy and capabilities at Los Alamos National Laboratory. Los Alamos began investigating photoelectric injectors to meet the low emittance, high peak current requirements for Free Electron Lasers (FELs), which could not be provided by conventional accelerator systems. Scientists at Los Alamos have helped pioneer photoelectric injector technology, from the original work of including photoemissive cathodes in rf cavities, starting in 1985,[1,2] to the design and construction of HIBAF, the first high brightness, high current (several hundred amperes) accelerator using a photoelectric injector, in 1989.[3]

This paper is broken into five sections. First, we will examine the choices for photoelectric injector design parameters that are available. Next, we will discuss the simulation and design procedures available for these choices. We will also provide a short description about the major physical processes involved in the injector, and why the emittance is lower than that of an injector based on a thermionic cathode. The last two sections will discuss higher frequency (>1 GHz) and lower frequency (<1 GHz) designs, respectively. Two separate high frequency designs will be presented, including the one used at HIBAF. Comparison with experimental measurements are provided for this design.

PHOTOELECTRIC INJECTOR DESIGN OPTIONS

Given typical accelerator gradients (twice the Kilpatrick electric field limit[4]) that can be sustained for pulse length formats suitable for FELs, and charges of 5 to 10 nC, there are two separate regimes for photoelectric injectors. The injectors can be designed either with accelerator frequency above or below 1 Ghz. The higher gradient available above 1 GHz allows use of phasing the laser pulse relative to the rf to provide some velocity bunching. This bunching as well as the rapid acceleration to relativistic velocity minimizes the axial electron pulse spreading due to the repulsive

space charge force. Final electron pulse lengths of 10 to 15 ps are possible for 5 nC. Although the high current in the pulse generates a large emittance growth due to the nonlinear space charge forces, the use of an external magnetic lens can virtually eliminate this emittance.[5] However, emittance contributions from both the nonlinear or linear but time varying rf fields can result in measurable emittances. The optimal lens placement becomes physically blocked for gradients much above 35 MV/m, and the space charge induced emittance compensation is less complete. Going to a higher frequency to make room for the lens is not satisfactory, since more emittance growth from the time varying rf forces also occurs. The optimum frequency for this type of design for 5 nC, 15 ps pulses is about 1.5 GHz.

The other type of photoelectric injector design assumes that we can bunch a longer electron pulse to 15 ps with only a small emittance growth, at worst. In that case, a sufficiently low accelerating frequency can be picked so there is only negligible rf emittance growth. Even with pulse lengths five times longer than the final desired length, the space charge induced emittance growth must be compensated. This emittance growth remains since the accelerating gradient also dropped with the frequency. The residual space charge induced emittance growth is also more dependent on the axial distribution of the bunch. At the appropriate frequency, only a small emittance remains after the compensation, and very little from the rf. If sufficient rf power is available to bunch at an arbitrary high energy, the emittance growth from the bunching process can also become negligible. Typically, though, rf power is limited, or the final energy is low (say 20 to 40 MeV) and a modest amount of emittance growth results. The brightness capable from either type of design is nearly the same.

DESCRIPTION OF SIMULATION CAPABILITIES

At Los Alamos we have developed the INEX [6] (Integrated Numerical EXperiment) approach to model the FEL system. In INEX, specific codes suited

for modeling different particular elements of the FEL system are linked together by passing from one to another the complete description of the electron beam. Typically 10^4 particles are followed in a simulation, and their entire phase space representation is passed from code to code. Various other codes are also used, to generate the appropriate external magnetic and rf fields the particle pushing routines need.

In particular, the FEL system can be broken into four sections. First, we define an injector system, to include up to the second rf cavity. The next section is the accelerator section, including beamline transport to the wiggler. The wiggler section is next, and followed by a final accelerator section which brings the beam to a dump. The main particle pushing codes used are ISIS,[7] PARMELA,[8] and FELEX.[9] FELEX pushes the particles in the wiggler, and includes the interaction with the light. Since we are concerned with high brightness accelerators only in this paper, we will not go into any more detail on FELEX.

ISIS is a fully 2-D Particle-in-Cell (PIC) code which solves Maxwell's equations for the rf and space charge fields, and uses the Lorentz force equation to push the particles. Except that it only supports 2-D effects, it is quite general. PARMELA is a very specific accelerator code. It uses external magnetic and rf field distributions generated by POISSON,[10] MAFIA,[11] and SUPERFISH,[12] which can include azimuthal effects. The Lorentz force equation is used to push the particles in these fields. Space-charge fields are calculated by making a relativistic transformation to an electrostatic frame, with an infinitely long conducting wall at the beam pipe radius. Effects of wake fields produced by the real wall opening into cavities is included by calculating the wake potentials from TBCI[12] and including it to the particles' energy after they leave the cavity.

The injector region is simulated by both ISIS and PARMELA, in order to get a feel for the accuracy of the simulation. Typically, they give practically identical results, including beam brightness.[3] Because ISIS requires full cavity description within its mesh, it can only include the first couple of accelerator cavities. The

accelerator section, including magnetic bends and bunchers, is simulated only by PARMELA, using TRACE to help tune up the focusing.

The accelerator modeling is quite sophisticated. We include in the simulation the effects of nonuniform transverse quantum efficiency maps, nonuniform transverse laser intensity, 3-D space charge effects, and 3-D cavity asymmetries from the coupling slots between accelerating cavities.

SPACE-CHARGE AND RF EMITTANCE GROWTH CONSIDERATIONS

The space charge emittance compensation technique by focusing with an external lens was developed at Los Alamos.[13] This technique simultaneously reduces the emittance as the beam envelope is focused (Fig. 1). The emittance reduction basically results from nonlinear space charge forces after the lens cancelling nonlinear space charge forces before the lens. The amount of compensation depends on how close the effective lens center approaches a particular location. This leads to a relatively small diameter of the lens to axially localize its field.

Since the beam pulse is not infinitely long, there are effects associated with the axial ends. The initial emittance growth is caused by nonlinear space charge forces which expand the beam at different rates at different axial positions. This causes a "bow-tie" to develop in phase space previous to the beam reaching the lens. The motion of the particles is phase space is at least quadratic; in general the motion is more complicated. The lens reinitializes their trajectories so that at some later time the "bow-tie" vanishes. This same thing can happen with no lens, if the right initial boundary conditions are used. Consider a drifting beam starting with

$$x = x_\circ$$

$$x' = -x'_\circ$$

Under a radial force of $\lambda v^2 m$, where the particle velocity is v and mass is m, the beam expansion is

$$x = x_\circ + \frac{\lambda}{2} z^2 - x'_\circ z$$

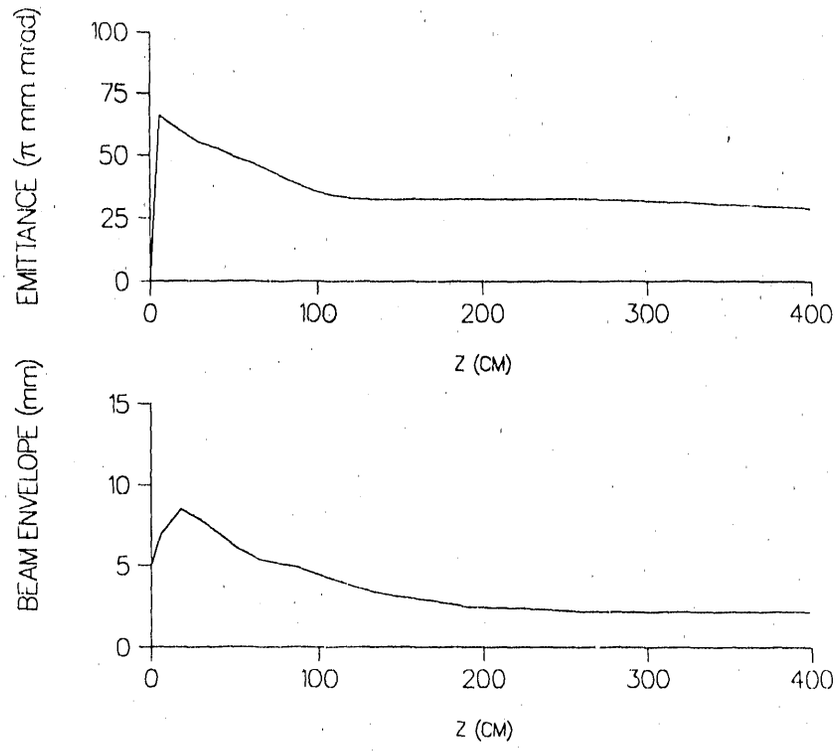

Fig. 1. Emittance and beam envelope size plotted against axial position.

$$x' = z\lambda - x'_o.$$

The angular width of the "bow-tie" is given by the spread of x'/x, given by

$$\frac{x'}{x} = \frac{z\lambda - x'_o}{x_o + \frac{\lambda}{2}z^2 - x'_o z}$$

which is in general a function of axial position within the bunch if λ is. If we pick

$$x'_o = x_o \frac{2}{z}$$

then

$$\frac{x'}{x} = \frac{2}{z}$$

independent of axial position, and the "bow-tie" has vanished. This effect is shown in Fig. 2 for a photoelectric injector and lens. Since the emittance is a quadratic, or

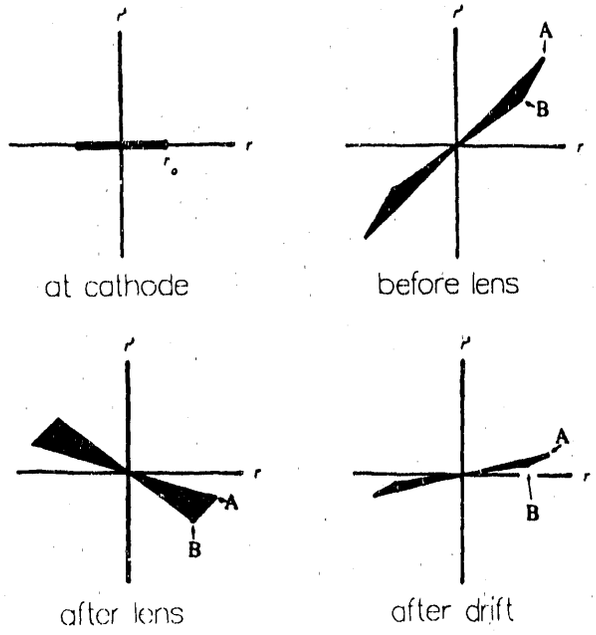

Fig. 2. Phase-space diagrams showing emittance reduction due to nonlinear space charge forces.

higher order, function of axial position,[14] it can be made to vanish at least at two axial location, for the proper boundary conditions.

In practice, not all space charge induced emittance can be eliminated. This occurs for the following reasons.

1. The space charge forces are originally radially nonlinear for short pulse lengths, and as the bunch lengthens they become axially nonlinear.
2. Particles at the bunch's axial ends often crossover, instead of forming a waist like the particles at the bunch's center.
3. Particles at the front of the bunch don't see the same space charge cloud before them as they leave the cathode as do the ones at the back end.

The amount of residual space-charge-induced emittance growth also depends on the initial pulse length and gradient. Longer pulse lengths lead to less emittance, because the average space-charge force has dropped, and because (1) above has been eliminated. Longer pulses are also more sensitive to axial distribution and require a

more uniform distribution. Higher gradients accelerate the particles faster, resulting in less time at the nonrelativistic energies where the nonlinear-space-charge forces cause emittance. However, as was pointed out earlier, the emittance that does occur is harder to compensate. Lower gradients are worse yet, because the beam distorts more from the space-charge forces and the emittance compensation suffers.

Electron pulses longer than ten degrees of rf phase tend to pick up emittance from the time variation in the rf fields. For pulses shorter than that, the main worry is radial nonlinearities in the fields. Since the emittance scales as the beam radius to the forth power, this can become quite large. Cavities with completely linear radial fields can be designed,[15] but they are unusable because of too low shunt impedance. On the other hand, cavities designed to maximize the shunt impedance have seriously nonlinear fields. Intermediate designs, with shunt impedances of three quarters the maximum, have only slightly nonlinear fields. These cavities are useful for beams up to 8 mm radius for 1 GHz. The different cavity shapes for 1.3 GHz and 1.2 cm beam pipe radius is shown in Fig. 3.

Depending on the availability of rf power, some trade offs are possible. If the electrons can be magnetically bunched at high (greater than 50 MeV) energy, and an initial uniform pulse can be generated, a very bright photoelectric injector can be made at frequencies less than 1 GHz. The initial pulse length can be increased, dropping the space-charged-induced emittance. Below 500 MHz, the space-charged-induced emittance starts to grow, resulting from the physical limitations of the nonlinear compensator.

HIGH FREQUENCY DESIGNS

We have two high frequency designs, both at 1.3 GHz for 5 nC electron bunches. The peak current, emittance, energy, and energy spread are outlined below:

The majority of this section will cover the HIBAF design; only differences introduced in the Advanced FEL (AFEL) design will be mentioned.

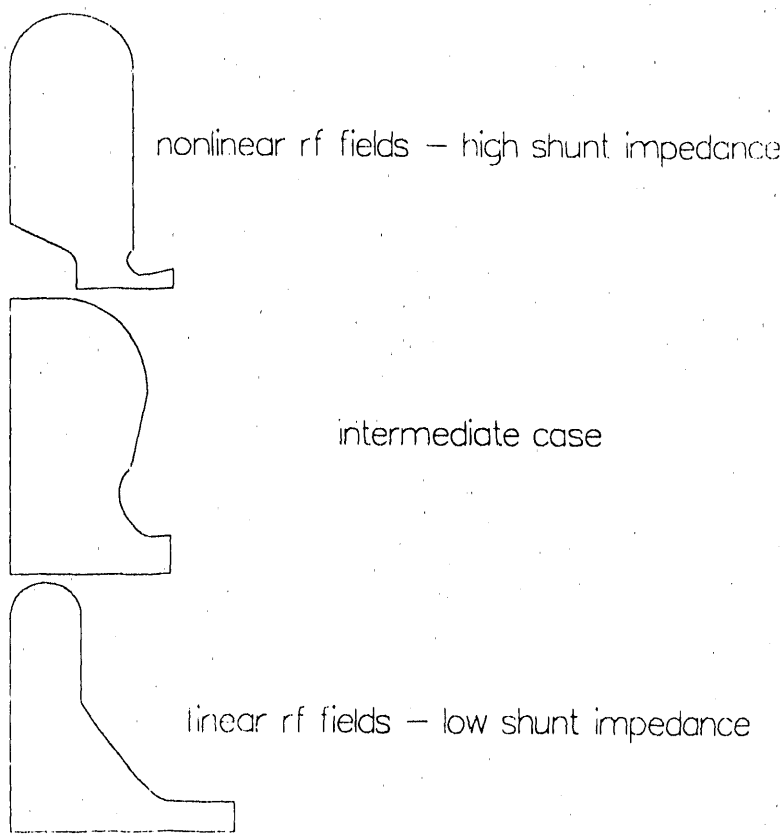

Fig. 3. Cavity shape selection trades off field linearity for shunt impedance.

Table 1

	I_{peak}	$\epsilon_{norm,90\%}$	$\frac{\Delta E}{E}$	Energy
HIBAF	320A	27π mm mrad	0.35%	40 MeV
AFEL	340A	12π mm mrad	0.20%	20 MeV

We will first review the HIBAF design philosophy, and its connection to the INEX procedure. The actual design and the INEX verification parameterization will also be covered. Current HIBAF status and experimental and INEX nominal case comparisons will be shown. One parameterization case will also be compared.

HIBAF was designed keeping all previous low emittance lessons in mind.[3] In particular, we wanted to:

1. Avoid all low energy beam drifts
2. Avoid axial mixing of the particles
3. Avoid wakefields, particularly in bends
4. Avoid beam loss near the cathode to prevent cathode poisoning

Part of the justification for building HIBAF was to verify the INEX design procedure for high current, low emittance machines. Many low emittance, low peak current accelerators exists. Accelerator optics are usually linear, and well understood. HIBAF is the first machine in the new regime of low emittance, high peak current, and there has been no previous benchmarking of the codes here. In particular, no device has previously been built with the correlated emittance compensator. In order to compare experimental and simulated results in this regime, a sophisticated understanding of the accelerator is required, as was discussed earlier. In particular, we want to use HIBAF to verify that the complicated nonlinear space charge forces calculated in INEX give essentially the right results. Although HIBAF is in the higher frequency, nonbunching regime, a magnetic buncher was designed in it, to verify the calculations in the lower frequency design.

HIBAF was designed to be maximally flexible, in order to do large parameterization studies. The wider the range of parameters that are within reach, the more regimes INEX could be tested in. In addition to the usual parameters easy to vary (charge, accelerator gradient, initial rf phase during emission, cathode radius, transverse beam profile, among others) variable amounts of radial rf focusing was provided, by changing the initial phase. The effective lens position for the compensator can also be changed, by varying the ratio of current in two separate coils.

In Fig. 4 we see the HIBAF master oscillator, power amplifier (MOPA)

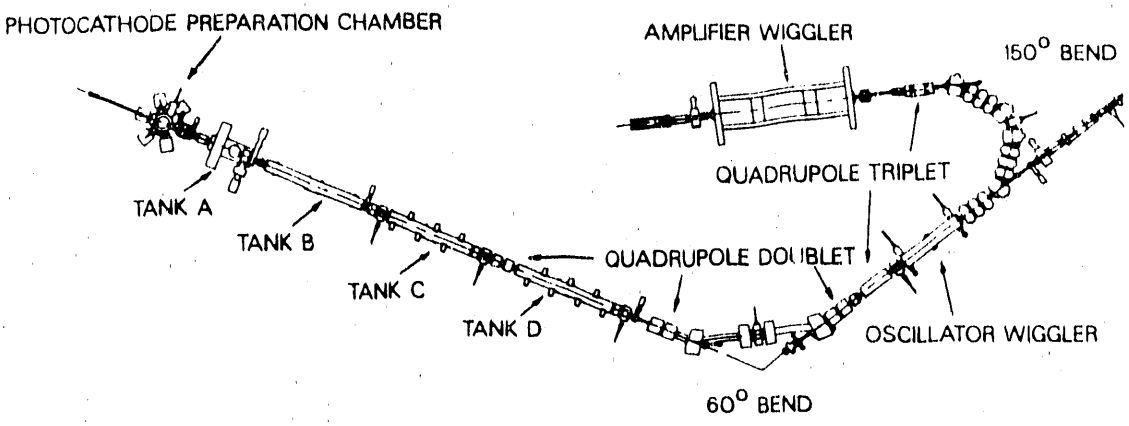

Fig. 4. HIBAF 40 MeV layout showing MOPA configuration.

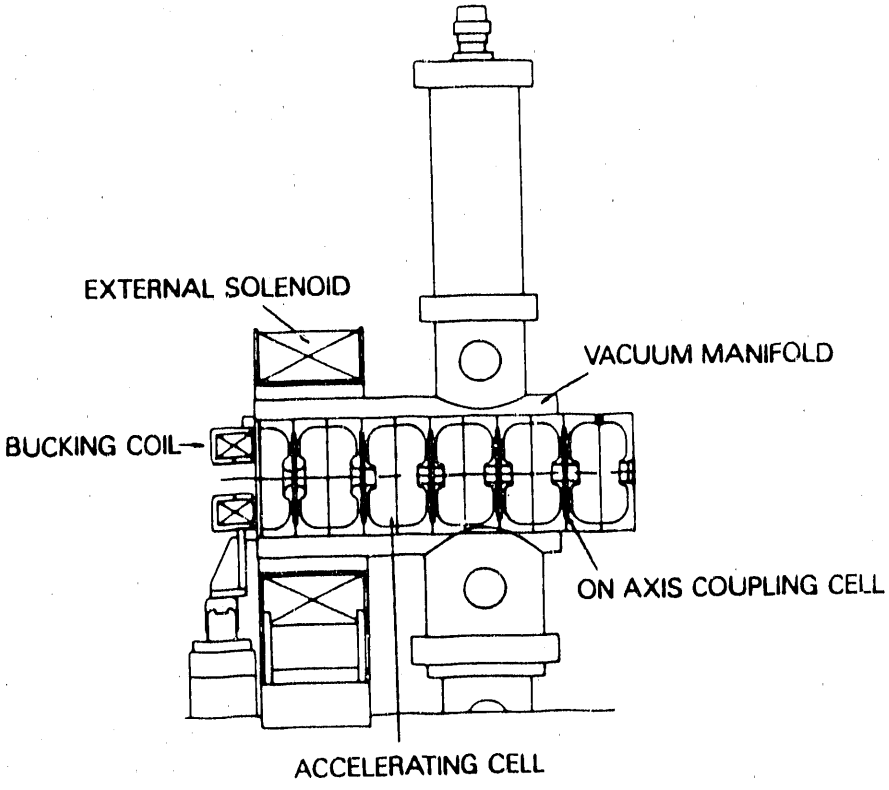

Fig. 5. HIBAF tank A showing on axis coupling cells and external lenses.

configuration. The accelerator consists of four standing wave tanks. The first tank, A, is an on-axis coupled structure with six cells (Fig. 5), and accelerates the beam 6 MeV. The other three tanks are side-coupled accelerators of 15 cells each, and accelerates the beam 11 MeV apiece. The final design energy is about 40 MeV. An isochronous and achromatic 60° bend transports the beam into the optical axis of an oscillator wiggler. A second, 150°, bend then guides the beam onto the optical axis of an amplifier wiggler. The secor bend can operate in both an isochronous and a nonisochronous manner.

Optical Transition Radiation (OTR) screens at locations 0,1,2, and 3 are available to measure the beam profile. Because of background subtraction issues and signal-to-noise resolution, beam full-width-half-max (FWHM) measurements are easier to make than are beam rms measurements.

The back wall of the first cell is recessed slightly (2.6 mm) at the cathode, to introduce some radial rf focusing, as the beam is accelerated. Another effect of the rf focusing is to drop the accelerating gradient at the cathode 25%.

Currently, HIBAF has only run as a 17 MeV machine (tanks C and D have not yet been installed). Fig. 6 shows a schematic of the 17 Mev machine. A nominal case has been established, and using the same tuning procedure, has been simulated.

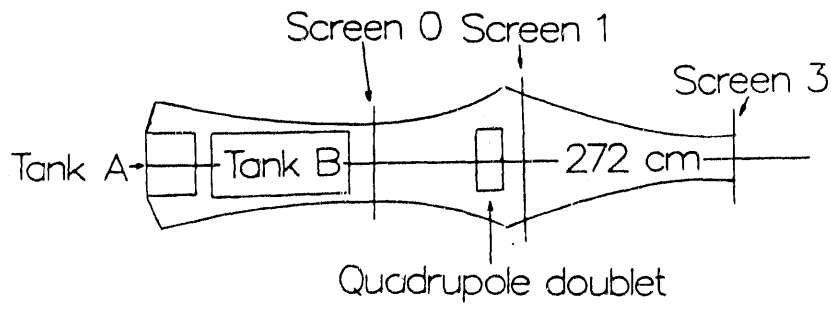

Fig. 6. HIBAF 17 MeV schematic, showing screen locations and beam envelope.

The nominal case is established by this tune-up routine:

1. With tank B detuned, measure the maximum acceleration through tank A with the spectrometer while varying the laser phase.
2. With tank B back on, measure the maximum acceleration with the spectrometer while varying the relative phase of A and B. This gives us the gradients of A and B to use in INEX.
3. Micropulse charge is determined from wall current monitors.
4. Electron pulse length measurements at the streak camera (located at screen 3) and initial laser pulse length measurements gives us the initial laser phase.
5. Relative rf phase of tank B is adjusted to minimize the energy spread.
6. Solenoid strength ratio is known experimentally; absolute strength is found by matching spot size on screen 0.
7. Ratio of quadrupole strengths is also known experimentally. Absolute strength is determined by minimizing beam spot size on screen 3.

There are only two free knobs available in the simulation setup - the solenoid and quadrupole strengths in steps 6 and 7. In Table 2 we see the summary of the nominal case, showing excellent agreement at all screens. The emittance for this case is 50 π mm mrad.

A crack in screen 0 interfered with the rms measurement. The HIBAF rms sizes were measured by fitting gaussian distributions to the data, and neglected the actual distribution wings that formed at the beam focus.

HIBAF parameterization studies have just begun. In this set of experiments, we plan to vary solenoid strength, cathode radius, micropulse charge and initial rf phase. These variations will check the INEX calculations of the nonlinear-space-charge compensator, the nonlinear-radial-space-charge force calculation, the nonlinear rf force calculation, and the effect for the rf focusing. In Fig. 7 we see

Table 2

	HIBAF	INEX
charge	3.6 nC	3.6 nC
energy	15.7 MeV	15.6 MeV
energy spread	0.3%	0.3%
peak current	180 A	200 A
pulse length	20 ps	20 ps
screen 0 FWHM x/y	2.8 mm / 3.5 mm	2.8 mm / 3.5 mm
screen 1 FWHM x/y	3.8 mm / 2.4 mm	3.4 mm / 2.1 mm
screen 3 FWHM x/y	0.82 mm / 1.32 mm	0.75 mm / 1.20 mm
screen 0 rms x/y	1.96 mm / 1.64 mm	2.0 mm / 2.3 mm
screen 1 rms x/y	2.2 mm / 1.0 mm	2.2 mm / 1.0 mm
screen 3 rms x/y	0.44 mm / 0.72 mm	0.58 mm / 2.5 mm

a plot of micropulse length versus initial rf phase, plotted from both experimental measurements and simulation. The agreement indicates that the interaction of the axial rf fields, radial rf fields, and the axial space charge fields is done to an acceptable accuracy in INEX, for this regime. By comparison with all the parameterization runs, agreement throughout the high current, high brightness regime will be examined.

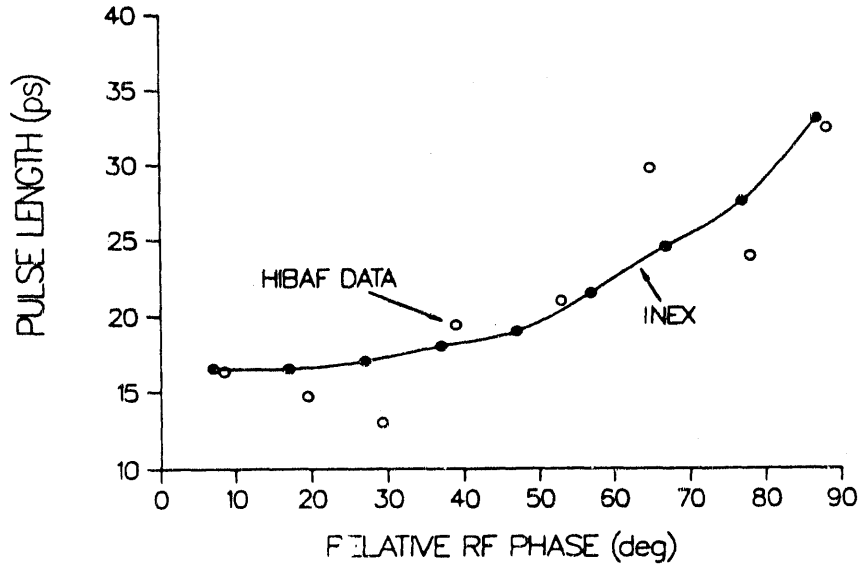

Fig. 7. Experiment and simulation comparison of micropulse length versus initial laser phase.

A brighter high-frequency linac can be designed, by removing the flexibility included in HIBAF. This requires that the necessary trust in INEX has been established by these verification experiments. The AFEL, shown in Fig. 8, consists of only one accelerator tank. Correct phasing of the rf to minimize the energy spread is provided by small additional drifts between accelerating cavities in the tank.

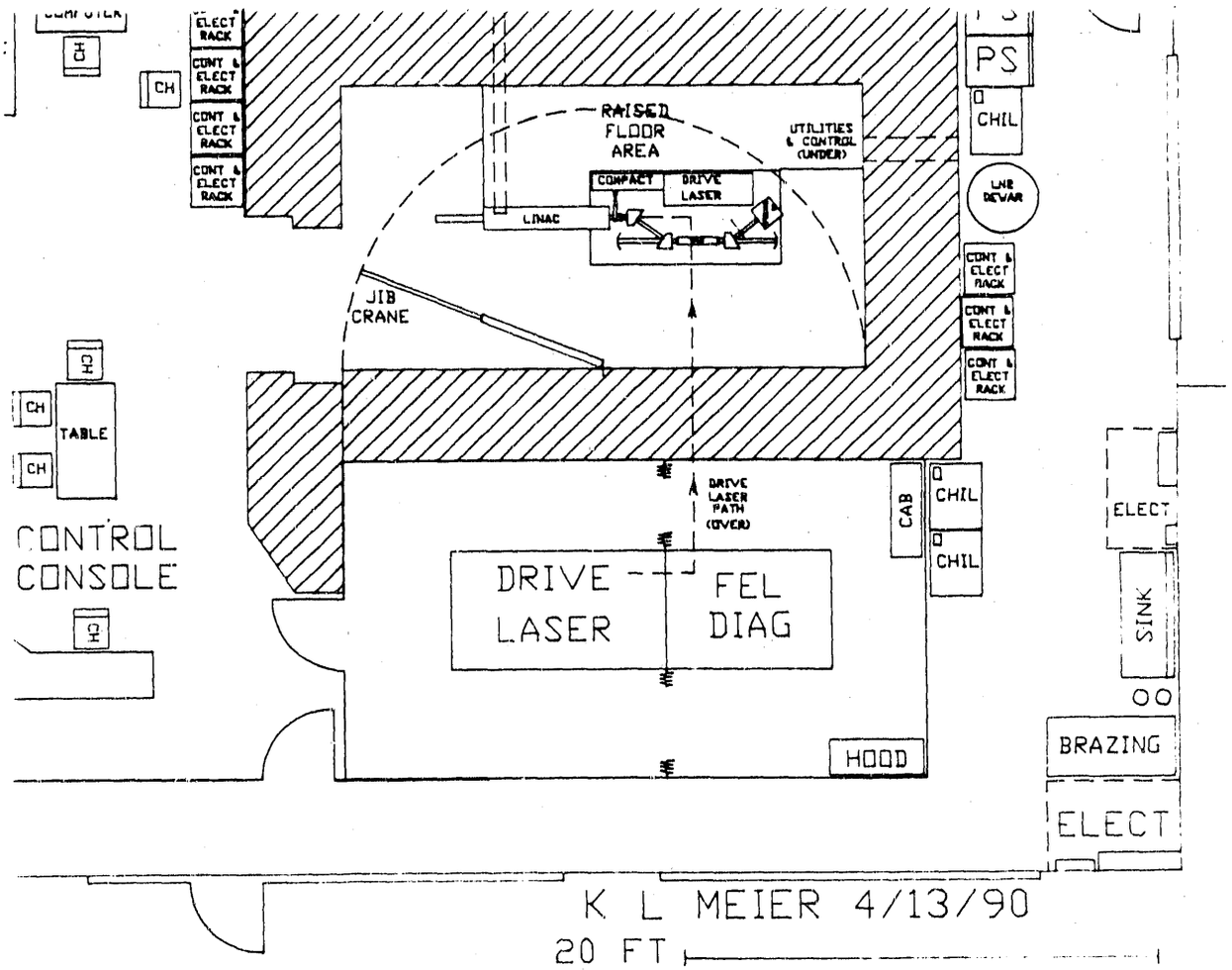

Fig. 8. Compact AFEL layout.

LOW FREQUENCY DESIGNS

In Table 3 we see a summary of a low frequency (433 MHz) photoelectric injector design shown schematically in Fig. 9.

Table 3

initial length 70 ps	25 π mm mrad
bunched to 10 ps	35 π mm mrad

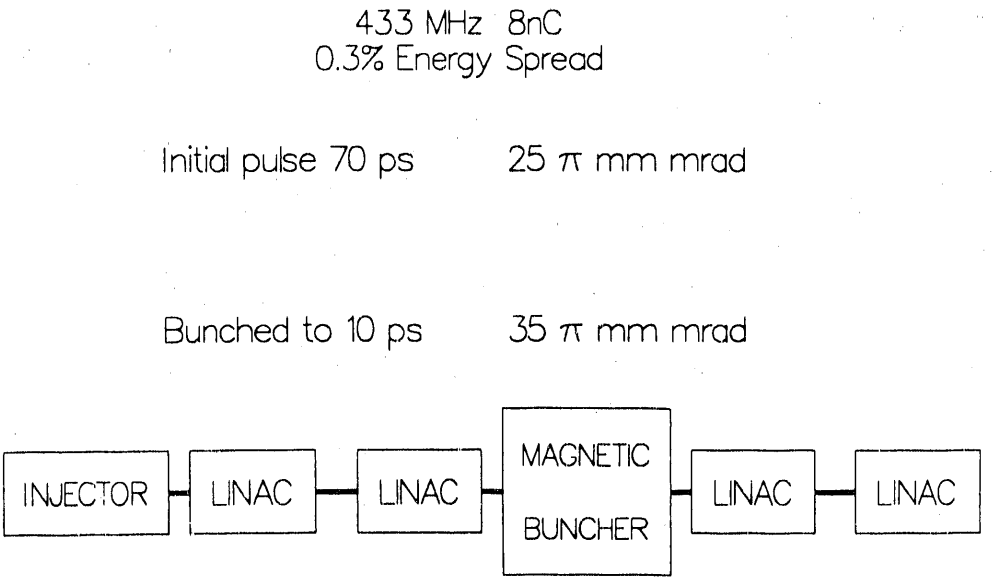

Fig. 9. Low frequency photoelectric injector schematic.

The 8 nC electron pulse was bunched at 22 MeV. The idea for a photoelectric injector below 1 GHz is different. Since the accelerating gradient is lower, a 10 ps, 5 nC pulse would blow apart to greater than 20 ps. In order to regain the high peak current, magnetic bunching is required. Depending on the rf power available and the final design energy, a trade off is now possible. At lower frequencies, a longer initial pulse can be used to minimize the space-charge-induced emittance growth. The penalty is that more magnetic bunching is needed. Even for pulse lengths

of 70 ps, the emittance compensator is needed to maintain high brightness. For frequencies less than a few hundred megahertz, the size of the first cavity starts to push the compensator away from the necessary location, and the emittance increases. An alternative is to drop the gradient below the twice Kilpatrick limit, but then additional emittance is generated, from violation of rule (1) of the HIBAF design.

In Fig. 10 we see the two classes of magnetic buncher; those with positive dispersion and those with negative dispersion. A typical example of each is shown. The dispersion is three times larger for the "circular" buncher than for the "chicane" one because the endpoints in the buncher where the trajectories of particles at different energies come together are closer. Either type of buncher will work, but they each have advantages.

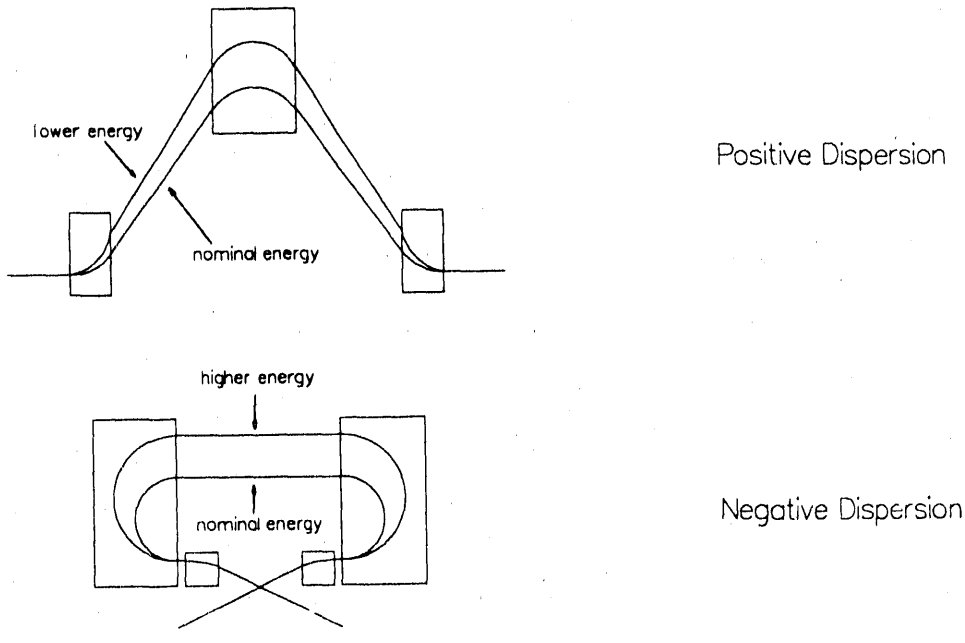

Fig. 10. Positive and negative dispersion magnetic bunchers.

The main emittance growth mechanisms in magnetic bunchers are nonlinear optics, radial space charge forces, axial space charge forces, and the potential

redistribution due to the bunching. The nonlinear optics refers to the order of nonachromaticity in the bend. Large energy spreads required for bunching over a short path length exacerbates this problem. Providing a high dispersion is important to keep this effect down.

The radial space charge force, which scales as one over gamma squared, effectively add in a defocusing lens within the bend. This can not be completely compensated for by focusing optics[16] within the bend as the space charge force varies axially along the bunch. This effect can be minimized by decreasing the path length within the compressor, and by focusing the beam to a waist in the final dipole.

The axial space charge force and the potential redistribution, which scale as one over gamma, lead to angular dispersion after the last dipole. This also is reduced by making the beam small there. In addition, the axial effect is make smaller by limiting the path length. The potential redistribution is independent of path length, but can be made uniform for the entire pulse. In that case, the final dipole just needs to be retuned to eliminate the emittance growth. These effects are discussed more completely in another paper.[17]

CONCLUSION

At Los Alamos, we have identified two separate regimes in which photoelectric injectors can operate for high brightness, high peak current devices. For electron charges of 5 nC, this corresponds to pulse lengths less than 15 ps and normalized emittances less than 40 π mm mrad. The first regime is where no magnetic bunching is used. The emittance is dominated by the nonlinear-space-charge forces. This design can operate between 1 and 1.5 GHz. Most of the emittance growth can be reduced with the correlated emittance compensator, but some is left. Higher frequency devices do not lead to less space-charge-induced emittance, until extremely high gradients ($>$ 200 MV/m) are achieved. Higher frequency devices also result in additional rf emittance growth. Lower frequency machines have lower accelerating

gradients, and both the space charge induced emittance growth increases and the peak current drops. Measurements at HIBAF are currently verifying the design tool INEX used in this regime.

A regime also exists in which we can magnetically bunch an initially longer pulse to 10 to 15 ps. In this regime the initial pulse length is long enough so that the space-charge-induced emittance is small after compensation. The emittance is then composed of rf effects and space charge effects in the magnetic buncher. The lowest reasonable frequency in this regime is around 400 MHz, for 5 nC. Lower frequencies start to physically restrict the amount of compensation possible. The emittance is more sensitive to the axial charge distribution in this regime.

Photoelectric injectors from either regime have comparable brightness. The design of both requires equal accuracy in the simulations. The higher frequency device depends on accurate space-charge field calculation at low energy. The lower frequency device needs just as accurate calculations of space-charge effects in the magnetic buncher.

ACKNOWLEDGMENTS

We wish to acknowledge helpful discussions with Lloyd Young and Lester Thode.

REFERENCES

1. J. S. Fraser, R. L. Sheffield, E. R. Gray, and G. W. Rodenz, "High-Brightness Photoemitter Injector for Electron Accelerators," IEEE Trans. Nucl. Sci. **32** (5), 1791 (1985).

2. M. E. Jones and W. Peter, "Particle-in-Cell Simulations of The Lasertron," IEEE Trans. Nucl. Sci. **32** (5), 1794 (1985).

3. B. E. Carlsten, L. M. Young, M. E. Jones, B. Blind, E. M. Svaton, K. C. D. Chan, and L. E. Thode, "Accelerator Design and Calculated Performance of the Los Alamos HIBAF Facility," Proc. 11th Int. Free-Electron Laser Conf., Naples, Florida, Aug. 1989, to be published.

4. W. D. Kilpatrick,"Criterion for Vacuum Sparking to Include Both RF and DC," Univ. of Ca. Rad. Lab., UCRL-2321(1953).

5. B. E. Carlsten, "Photoelectric Injector Design Code," Proc. 1989 IEEE Particle Accelerator Conf., IEEE Catalog No. 89CH2669-0, 133(1989).

6. J. C. Goldstein, B. D. McVey, B. E. Carlsten, and L. E. Thode, "Integrated Numerical Modeling of Free Electron Laser Oscillators," Nucl. Instr. and Methods in Physics Res. **A285**,192 (1989).

7. G. Gisler, M. E. Jones, and C. M. Snell, "ISIS: A New Code for PIC Plasma Simulations," Bull. Am. Phys. Soc. **29**,1208(1984).

8. L. M. Young, Los Alamos National Laboratory, private communication.

9. B. D. McVey, "Three-Dimensional Simulations of Free Electron Laser Physics," Nucl. Instr. and Meth. **A250**,449(1986).

10. K. Halbach, R. F. Holsinger, W. E. Jule, and D. A. Swenson, "Properties of the Cylindrical RF Cavity Evaluation Code SUPERFISH," Proc. 1976 Proton Linear Accel. Conf., Chalk River Nucl. Lab. report AECL-5677, 122(1976).

11. R. Klatt, F. Krawczyk, W. R. Novender, C. Palm, T. Weiland, B. Steffen, T. Barts, M. J. Browman, R. Cooper, C. T. Mottershead, G. Rodenz, and S. G. Wipf, "MAFIA- A Three-Dimensional Electromagnetic CAD System for Magnets, RF Structures, and Transient Wake-Field Calculation," Proc. 1986 Linear Acc. Conf., SLAC report SLAC-303, 276(1986).

12. T. Weiland, "Transverse Beam Cavity Interaction, Part I: Short Range Forces," Deutsches Electronen-Synchrotron report DESY 82-015(1982).

13. B. E. Carlsten, "New Photoelectric Injector Design for the Los Alamos National Laboratory XUV FEL Accelerator," Nucl. Instr. and Methods in Physics Res. **A285**,313 (1989).

14. B. E. Carlsten and R. L. Sheffield, "Photoelectric Injector Design Considerations," Proc. 1988 Linear Acc. Conf., CEBAF-Report-89-001 (1989).

15. K. T. McDonald, "Design of the Laser-Driven Radio Frequency Electron Gun for the Brookhaven Accelerator Test Facility," Princeton University Report No. DOE/ER/3072-43.

16. A. J. Jason, E. M. Svaton, B. Blind, and E. A. Heighway, "Design of Achromatic Bending Systems in the Presence of Space Charge," Proc. 1987 IEEE Particle Accelerator Conf., IEEE Catalog No. 87CH2387-9, 1767(1987).

17. B. E. Carlsten, B. D. McVey, E. M. Svaton, and L. M. Young, "Magnetic Bunchers for the Generation of High Peak Current, Low Emittance Electron Pulses at Medium Energy," Proc. 1990 Linear Acc. Conf., Albuquerque, NM, Sept 1990, to be published.

END

DATE FILMED

10 / 25 / 90